Published in final edited form as:
Neuron. 2014 March 19; 81(6): 1375–1388. doi:10.1016/j.neuron.2014.01.024.

NMDA RECEPTOR ACTIVATION STRENGTHENS WEAK ELECTRICAL COUPLING IN MAMMALIAN BRAIN

Josef Turecek[1], **Genevieve S. Yuen**[2], **Victor Z. Han**[3], **Xiao-Hui Zeng**[3], **K. Ulrich Bayer**[4], and **John P. Welsh**[3,5]

[1]Department of Neurobiology, Harvard Medical School, 220 Longwood Ave., Boston MA 02115

[2]Department of Psychiatry, New York Presbyterian Hospital-Weill Cornell Medical College, 525 East 68th St., New York, NY 10065

[3]Center for Integrative Brain Research, Seattle Children's Research Institute, 1900 9th Avenue, Seattle WA 98155

[4]Department of Pharmacology, University of Colorado-Denver School of Medicine, 12800 E. 19th Ave., Aurora CO 80045

[5]Department of Pediatrics, University of Washington, 1959 NE Pacific St., Seattle WA 98195

SUMMARY

Electrical synapses are formed by gap junctions and permit electrical coupling that shapes the synchrony of neuronal ensembles. Here, we provide the first direct demonstration of receptormediated strengthening of electrical coupling in mammalian brain. Electrical coupling in the inferior olive of rats was strengthened by activation of NMDA-type glutamate-receptors (NMDARs), which were found at synaptic loci and at extrasynaptic loci 20–100 nm proximal to gap junctions. Electrical coupling was strengthened by pharmacological and synaptic activation of NMDARs, while co-stimulation of ionotropic non-NMDAR glutamate-receptors transiently antagonized the effect of NMDAR activation. NMDAR-dependent strengthening (i) occurred despite increased input conductance, (ii) induced Ca^{2+}-influx microdomains near dendritic spines, (iii) required activation of the Ca^{2+}/calmodulin-dependent protein-kinase II, (iv) was restricted to neurons that were weakly coupled, and thus, (v) strengthened coupling mainly between non-adjacent neurons. This provided a mechanism to expand the synchronization of rhythmic membrane potential oscillations by chemical neurotransmitter input.

Correspondence john.welsh@seattlechildrens.org.

The authors declare they have no conflicts of interest.

INTRODUCTION

There are two well-known mechanisms in mammalian brain that allow chemical synaptic transmission to modulate electrical synaptic transmission between neurons. Both are inhibitory. The first mechanism was observed in the adult inferior olive (IO), where the opening of chloride channels triggered by GABA receptor activation increased the input conductance and thereby shunted current away from the site of dendritic gap junctions (GJs; Lang et al., 1996; Llinás et al., 1974), an evolutionarily conserved mechanism for electrical uncoupling first described in the mollusc *Navanax inermis* (Spira and Bennett, 1972). The second mechanism was observed in the early postnatal thalamus where metabotropic glutamate receptor activation produced long-term inhibition of electrical synapses (Landisman and Connors, 2005). Both mechanisms provide a means by which chemical synapses can attenuate synchronous activity within neuronal ensembles.

Evidence for chemical synaptic transmission that strengthens electrical synapses in mammals would be important because it would explain a means of upregulating synchronous activity. Despite decades of research, such a mechanism has not been demonstrated in mammalian brain. A study of motoneurons in the mollusc *Aplysia californica* revealed strengthening of electrical coupling by chemical synaptic input that decreased potassium conductance and reduced current shunting through the non-junctional membrane (Carew and Kandel, 1976). A study of the VIIIth-nerve synapse in teleost fish brainstem found that activation of postsynaptic NMDA-type glutamate receptors (NMDARs) strengthened an adjacent electrical synapse made by the same nerve terminal (Pereda and Faber, 1996; Pereda et al., 1998). NMDAR activation enhanced tracer-coupling among AII amacrine cells (Kothman et al., 2012), an anatomical measure of GJ patency that can sometimes relate indirectly to electrical coupling. Yet, whether activation of a chemical synaptic receptor can strengthen electrical coupling in the mammalian brain remains unsubstantiated.

The IO is an excellent system for studying electrical synapses in mammalian brain (Llinás et al., 1974; Sotelo et al., 1974). It has the highest density of GJs in the adult brain and the properties of its electrical synapses are well described. GJs are formed by transmembrane channels comprised of connexin36 (Cx36) protein (Condorelli et al., 1998). Electrical synapses between IO neurons are made within clusters of 5–6 dendritic spines coupled by GJs; these clusters of spines are surrounded by synaptic boutons and astrocytic processes to form the olivary glomerulus (Sotelo et al., 1974). The synaptic boutons are composed of a nearly equal ratio of GABAergic and glutamatergic terminals, the former originating from the deep cerebellar nuclei and the latter from the midbrain (De Zeeuw et al., 1989, 1990). Each IO neuron may be electrically coupled to at least 50 other neurons (Devor and Yarom, 2002). Despite the prevalence of electrical coupling, the gap junctional conductance (G_j) between coupled IO neurons has a mode less than 100 pS (Hoge et al., 2011), which is lower than for any other electrically-coupled system in the adult brain.

Weak electrical coupling in the IO provides a low baseline upon which a strengthening mechanism could operate to have significant functional effect. Electrical synapses between IO neurons have two functions: 1) to synchronize the output of the nucleus in order to drive

synchronous postsynaptic responses in cerebellar Purkinje cells (Llinás and Sasaki, 1989; Welsh et al., 1995) and 2) to strengthen and synchronize the 2–12 Hz oscillations in membrane potential that are subthreshold for spiking (Llinás and Yarom, 1986). Subthreshold oscillations (STOs) function as a carrier rhythm that determines moments at which synaptic input can have greater or lesser probability of triggering an action potential. Genetic knockdown of Cx36 in the IO blocked coupling and reduced the synchrony (Long et al., 2002), amplitude, and continuity (Placantonakis et al., 2006) of STOs, thereby increasing variability in spike timing within the cerebellum (Van der Giessen et al., 2008). The findings that uncoupling desynchronized and weakened STOs suggested that strengthening electrical coupling would synchronize and strengthen STOs.

Our experiments examined mechanisms whereby NMDAR activation synchronizes brain activity. We first described the spatial relation of NMDARs to Cx36 within IO dendrites by using 3-dimensional confocal microscopy and, thereafter, a pool of extrasynaptic NMDARs adjacent to GJs by using thin-section immunotransmission electronmicroscopy (TSIEM). We used dual patch-clamp recordings to directly demonstrate that NMDAR activation synchronizes STOs and strengthens weak electrical coupling. We established physiological relevance by showing that synaptic excitation strengthened weak electrical coupling and used rapid 2-photon (2-p) imaging to implicate microdomains of synchronized Ca^{2+} influx near dendritic spines of electrically-coupled neurons during NMDAR activation. Our study revealed mechanisms whereby NMDAR activation strengthens electrical synapses in order to synchronize neuronal activity.

RESULTS

NMDARs near neuronal GJs

IO neurons were transduced to express green fluorescent protein (GFP; Placantonakis et al., 2006) and processed using double label immunohistochemistry for the NR1 subunit of the NMDAR and Cx36 (Figure 1). Confocal microscopy revealed that neuropilar NR1 and Cx36 immunopuncta were often spaced less than 1 μm and had a mode spacing of 125 nm (n=1133; Figure S1). Twenty-six percent of pairs of Cx36 puncta within 1 μm were contiguous and among contiguous Cx36 puncta (n=89), 71% showed one or two NR1 puncta immediately adjacent. The result was a triple- or quadruple-assembly in which two Cx36 puncta spaced 415 ± 7 nm apart were flanked by one or two NR1 puncta offset by 225 ± 11 nm. Of note was that 10% of NR1 puncta in Cx36-NR1 pairs resided only 20–100 nm away from a Cx36 signal. Surface rendering and 3-dimensional reconstructions of IO dendrites revealed Cx36-NR1 quadruple assemblies within adherences linking two dendrites running in parallel, consistent with their being positioned to play a role in GJ coupling (Figure 1). Also within the dendritic adherences and confluent dendritic shafts were Cx36-NR1 pairs not configured into assemblies as well as unpaired Cx36 and NR1 puncta.

We used TSIEM to visualize the relation between GJs and membrane-localized NR1 which could not be resolved with light microscopy. GJs were identified by the narrowing of the intermembrane space to approximately 20 nm within glomeruli of apposed dendritic spines and interdigitated chemical synaptic terminals (Sotelo et al., 1974). The length of GJs in the rat IO was 285 ± 27 nm, similar to mouse (272 ± 26 nm; De Zeeuw et al., 2003). TSIEM

replicated a previous finding (Hoge et al., 2011) that NR1 within postsynaptic densities (PSDs) resided 300–500 nm from GJs, but also revealed a previously unidentified pool of extrasynaptic NR1 immunopuncta 20–100 nm proximal to GJs.

Figure 2 shows three examples. In a first example (Figure 2A), an axon terminal (T) made excitatory chemical synapses onto two spines (asterisks) with each glutamatergic PSD containing NR1 immunoreactivity (arrows next to asterisks). One of the dendrites (d1) that received the synaptic input was coupled to another dendrite (d2) via a GJ and expressed an NR1 on the membrane only 87 nm from the GJ (Figure 2B). This NR1 expression was "extrasynaptic" using the criterion that its distance from a PSD exceeded 300 nm (Petralia et al., 2010). The coupled dendrite (d2) also expressed NR1 near the GJ but slightly away from the membrane in the cytosol (arrow in d2). In a second example (Figure 2C), 3 dendrites (d1, d2, d3) were organized in series and showed membrane appositions characteristic of GJs (arrowheads). All 3 dendrites expressed NR1 in their cytosol or plasmalemma membrane. Two extrasynaptic NR1s in the membrane (arrows, Figure 2C) were positioned 27 and 69 nm from GJs (arrowheads, Figure 2C,D). In a third example (Figure 2E), 4 dendritic spines and 3 terminals were present in a glomerulus. The 4 spines were separated into coupled pairs (d1/d2 and d3/d4). All 4 spines expressed NR1 and an extrasynaptic NR1 was present on the membrane of d2 about 10 nm from a GJ. Again, a cytosolic NR1 within d1 was close to a second GJ (arrow). The anatomy motivated the following experiments.

NMDAR activation synchronizes STOs

Pairs (N=197) of IO neurons with somata spaced closer than 100 μm were recorded in whole-cell mode using two patch clamp electrodes. Their identity as IO neurons was confirmed by their intrinsic membrane properties under current- and voltage-clamp and in some cases also by their morphology (Figure S2).

As it has been shown that GJs synchronize STOs, a subset of the pairs (n=42) was used to determine the effect of NMDAR activation on STO synchrony. On average, NMDA depolarized the membrane of IO neurons from −59.9 ± 0.9 to −54.4 ± 1.0 mV. The majority of pairs (83%) showed synchronized STOs during NMDA and was divided into 4 groups (Figure 3). A common behavior (33% of pairs) was that STO synchrony was maintained during NMDA (Figure 3A). A second behavior (45%) was that neither neuron oscillated before NMDA but showed synchronized STOs during NMDA (Figure 3B). A third behavior (5%) was that STOs were out of phase before NMDA but synchronized by NMDA (Figure 3C). The remaining 17% also depolarized but were non-oscillatory and showed no STOs both before and during NMDA (No-STO group). The intersomatic distance of the cell pairs of each group averaged between 25 and 27 μm (mode 15 μm) with the exception of the group whose STOs were out of phase prior to NMDA which averaged 67 μm. An increase in STO amplitude from 8.7 ± 1.5 to 10.5 ± 1.7 mV occurred in 50% of the neurons treated with NMDA. Among synchronously spiking IO neurons, with or without NMDA, the number of axonal spikes detected in the soma was inversely proportional to STO amplitude (Bazzigaluppi et al., 2012b, De Gruijl et al., 2012; Figure S2). The No-STO group served as an important control for the effect of NMDAR activation on coupling independent of oscillation (below). In sum, the experiment showed that an important result of NMDAR

activation was STO synchronization, consistent with an enhancement of GJ coupling and motivating studies of electrical coupling.

NMDAR activation strengthens electrical coupling

Electrical coupling strength was measured by calculating coupling coefficients (CCs). CCs were determined by injecting negative current into each neuron and calculating the ratio of the steady-state voltage response of the non-injected cell to that of the current-injected cell (Devor and Yarom, 2002; Hoge et al., 2011). A challenge in measuring CCs of electrically-coupled, oscillating neurons was that STOs conducted through GJs obscured the steady-state voltage responses needed to measure CCs. Thus, we applied nifedipine or a cocktail of $NiCl_2$ and CsCl to block both intrinsic and NMDA-induced STOs (Best and Regehr, 2009, Placantonakis and Welsh, 2001) prior to measuring CCs. Blocking STOs did not significantly affect the pre-NMDA CC as compared to the baseline CC of the No-STO group which could be measured without blockers (Figure S3). Moreover, blocking STOs with nifedipine or Ni/Cs did not alter mean CC during NMDAR activation as compared to the mean CC of the No-STO group during NMDAR activation. This allowed experiments in which the effect of NMDAR activation on electrical coupling could be measured independent of its effect on STOs.

Figure 4A shows the paradigm. In this example, before NMDA weak electrical coupling was observed in response to current injected into either cell, with CC_{AB} and CC_{BA} both being 0.5%. NMDA depolarized the neurons and increased CC_{AB} to 1.3% and CC_{BA} to 1.8%, demonstrating a strengthening effect. Analyses of coupling strength were performed in 89 cell pairs that were coupled as defined by a voltage deflection of at least 0.03 mV in response to −300 or −500 pA current injection in the neighboring neuron (Devor and Yarom, 2002). Under normal conditions (n=82 pairs, Figure 4B), CC values fell from 1.2 ± 0.1% when cells were 16 ± 1 μm apart (n=40 pairs) to 0.6 ± 0.1% when cells were 75 ± 2 μm apart (n=16 pairs). The reduction in CC with increasing intersomatic distance replicated a previous report (Devor and Yarom, 2002). In 48 pairs of neurons coupled while 50 μM NMDA was added, the distancecoupling function was skewed to the right due to an increase in CC over intersomatic distances of 30–60 μm (Figure 4B).

Figure 4C plots the percentage change in CC as a function of intersomatic distance for 31 cell pairs in which electrical coupling was measured both before and during NMDA. There was a non-uniform relationship between the change in CC over intersomatic distances of 10 to 100 μm with increases of 43 ± 11% at 10 μm, 105 ± 19% at 30 μm, 93 ± 30% at 60 μm, and 34 ± 11% at 90 μm. The non-uniform change in CC over intersomatic distance accounted for the rightward skewing of CC with distance during NMDAR activation (Figure 4B). The strengthening of electrical coupling by NMDA allowed non-adjacent neurons separated by up to 50 μm to have CCs nearly as strong as those that were directly adjacent before NMDA. As previously reported (Devor and Yarom, 2002), the two directions of CCs in pairs of IO neurons were not always equal under baseline conditions leading sometimes to significant asymmetry of coupling. In our sample, coupling strength between directions among the same cell pair could differ by as much as 1.6% in raw CC. Figure 4D demonstrates that NMDAR activation had strong effects on coupling symmetry that varied

greatly. In some pairs, NMDAR activation nearly completely reversed coupling asymmetry while in other pairs it induced significant asymmetry. Overall, NMDAR had no net effect on coupling asymmetry (CC difference of 0.5 ± 0.1% baseline *vs*. 0.6 ± 0.1% NMDA).

We tested the time course of NMDA's effect on electrical coupling (Figure 4E). In 8 pairs (mean distance 39 ± 8 μm), NMDA increased the mean CC from 1.0 ± 0.1% to 1.2 ± 0.1% after 10 min exposure to NMDA ($p < 0.01$). Upon removing NMDA CCs returned to the baseline within 5 min, a time-course of recovery similar to that following the strengthening of coupling in the teleost VIIIth-nerve Mauthner cell synapse (3 min, Pereda and Faber, 1996) and having similar effect of doubling coupling strength at the most sensitive intersomatic distance.

NMDAR activation increases coupling probability and GJ patency

Analyses of the effect of NMDAR activation on the probability of electrical coupling in IO neurons were carried out in 107 cell pairs. Using the definition of Hoge et al. (2011), the presence of electrical coupling was a CC value of at least 0.5% (Figure 5A). The probability of electrical coupling was 80% at intersomatic distance of 0–20 μm but only 18% at 61–80 μm (Figure 5B). NMDAR activation increased coupling probability at all distances but had its greatest effect among neurons separated by 41–60 μm ($p < 0.01$; Figure 5B). In those pairs, NMDAR activation increased coupling probability from 47% to 93%, a value equivalent to the coupling probability of adjacent neurons prior to NMDA.

We tested whether the enhancement in coupling probability may have been due to an increase in GJ patency using transmembrane diffusion of Neurobiotin. Under control conditions (n=8), intracellular injection of Neurobiotin into IO neurons produced an average of 8.0 ± 1.7 tracer-coupled cells, within the range of previous reports (3.9, Devor and Yarom, 2002; 7.8, Placantonakis et al., 2006; 12.5, Hoge et al., 2011). Repeating the injections (n=7) during NMDAR activation and subsequently bathing the slices in 30 μM NMDA before fixation produced an average of 16.1 ± 1.6 tracer-coupled cells, twice as many as the controls and exceeding previously published values ($p < 0.05$; Figure 5C,D). To measure the spatial distribution of the change, we counted the number of tracer-coupled neurons in concentric 20 μm-wide rings around the soma of the injected neuron. NMDA produced the greatest increase in tracer-coupling at 40–60 μm (Figure 5E), mirroring the spatial enhancement in the probability of electrical coupling found by electrophysiology (Figure 5F).

Specificity for weak electrical coupling

To address mechanism, we first subdivided all of the pre-NMDA measurements into CC directions that represented strong (≥ 2% CC, n=13), moderate (1.01 to 1.99% CC, n=15), and weak coupling (0.5 to 1% CC, n=42). NMDAR activation strengthened weak (0.6 ± 0.1 to 1.0 ± 0.1% CC; $p < 0.01$) and moderate (1.3 ± 0.1 to 1.8 ± 0.2% CC; $p < 0.05$) coupling, but did not affect strong coupling (from 2.9 ± 0.3 to 2.6 ± 0.4% CC).

NMDA strengthening of electrical coupling was receptor mediated. The coupling of weakly and moderately coupled neurons was not strengthened by NMDA when they were pretreated

with MK-801, a non-competitive antagonist of the NMDAR channel (Figure 6A). In addition, weak and moderate coupling was nearly abolished by agonists of other ionotropic glutamate receptors. This was determined by bath applying 2-amino-3-(3-hydroxy-5-methyl-isoxazol-4-yl)propanoic acid (AMPA) or kainate (KA). AMPA and KA depolarized neurons by 16.1 ± 1.9 mV and 18.8 ± 4.5 mV, respectively and significantly reduced CCs by 72 ± 7% ($p < 0.05$; Figure 6B). In addition, AMPA and KA never induced STOs and always abolished them.

Calculations of the GJ and input conductances (G_j and G_{in}) indicated that the strengthening of coupling may have resulted from direct modulation of G_j. A change in Gj may be due to a change in the passive properties of the non-junctional membrane such as membrane leakiness and/or due to direct modulation of the GJ protein. If the increase in electrical coupling during NMDA followed a reduction in the leakiness of the non-junctional membrane (Carew and Kandel, 1976), then an increase in G_j should have been associated with a decrease in G_{in} during NMDA. In fact, the opposite relation was found. During NMDA, the increase in G_j scaled positively with an increase in G_{in} (Figure 6C, n = 31 pairs). This relationship was true only for weakly- and moderately- coupled neurons. A strong shunting effect to reduce G_j was observed during treatment with AMPA and KA (n = 8 pairs), accounting for the significant reduction in CC they produced. Thus, weakly and moderately coupled neurons were unique in showing an increase in G_j with increased G_{in}, indicating a potential role for NMDAR activation to directly modulate the GJ.

Necessity of CaMKII

CaMKII has been implicated as an important downstream mediator of NMDAR-induced Ca^{2+} signaling (Coultrap and Bayer, 2012). To examine the role of CaMKII in the NMDAR strengthening of electrical coupling, we performed experiments with two different CaMKII inhibitors: KN-93, which was bath-applied (Figure 6D, top); and tatCN21 peptide, which was dissolved into the internal solution of the two electrodes and thus restricted to two electricallycoupled neurons (Figure 6D, bottom).

Bath application of KN-93 to weakly coupled pairs (n=4) had no effect on baseline CCs (pre KN-93, 0.8 ± 0.1%; KN-93, 0.6 ± 0.2%) but completely blocked the NMDA-induced strengthening of coupling ($p < 0.05$; KN-93+NMDA, 0.5 ± 0.2% CC; Figure 6E). Because KN93 does not discriminate among various CaMKs (Enslen et al., 1994) and affects also voltage-gated Ca^{2+} and K^+ channels (Gao et al., 2006; Ledoux et al., 1999), we next tested tatCN21, a CaMKII-specific peptide inhibitor (Vest et al., 2007). While KN93 blocks activation by Ca^{2+}/calmodulin, the 21-amino acid peptide tatCN21 blocks substrate access, adding the advantage of utilizing two mechanistically distinct inhibitors.

Including tatCN21 into the internal solution of the electrodes also blocked the strengthening of weak and moderate electrical coupling by NMDA ($p < 0.05$; n=6 pairs, Figure 6F). The mean pre-NMDA CC during dual intracellular tatCN21 was 1.0 ± 0.1% and subsequent NMDAR activation induced no change (tatCN21+NMDA, 0.8 ± 0.2% CC). To control for the dialysis of an exogenous peptide, the experiment was repeated using tatCtrl, a scrambled sequence control peptide (Vest et al., 2007). TatCtrl did not block NMDA from strengthening CCs in weakly coupled neurons (tatCtrl, 0.5 ± 0.1% CC; NMDA+tatCtrl, 0.9

± 0.1% CC, n=5 pairs). Intracellular blockade of CaMKII with tatCN21 nearly always blocked NMDA-induced STOs as opposed to pairs with intracellular tatCtrl (Figure 6G). Thus, CaMKII blockade: 1) blocked the strengthening of weak electrical coupling by NMDA, and 2) prevented the induction of STOs by NMDA in cells that were quiescent prior to NMDA.

Synaptic activation of NMDARs strengthens electrical coupling

To determine whether strengthening of electrical coupling could be induced by synaptic activation, we tested the effect of 3 patterns of synaptic input triggered by electrical stimulation of the reticular formation (Figure 7A). Since previous studies of the neonatal thalamus demonstrated that tetanic burst stimulation depressed electrical coupling via glutamatergic neurotransmission (Landisman and Connors, 2005), we began by using 50 Hz burst stimulation. Under normal ACSF (n=7), such bursts evoked sequential EPSPs riding on an envelope of membrane depolarization (peak 7.0 ± 0.7 mV) which depressed during each train (Figure 7B). Weak electrical coupling was not strengthened by 4 min of burst stimulation (9 ± 13% increase in CC). Because burst stimulation was shown to bias GABAergic terminals to release within the IO (Best and Regehr, 2009) and may have also caused significant release from a dense local network of 5-HT fibers, we repeated the experiment using slow paired-pulse stimulation (PPS, Figure 7C). Following 4 min of PPS (n=8), weak electrical coupling was significantly strengthened by 25 ± 10% ($p < 0.05$). To test receptor specificity, in a different set of neuron pairs (n=7) pre-treating with MK-801 occluded CC strengthening by PPS.

The increase in CC following PPS occurred without block of AMPARs whose coincident activation would be expected to increase G_{in} and counterbalance the strengthening induced by NMDAR activation. To determine the contribution of AMPARs to the modulation of CCs and to maximize the activation of extrasynaptic NMDARs, we lengthened the stimulus train to 500 ms, decreased pulse frequency to 9 Hz, removed Mg^{2+} from the ACSF, and varied AMPAR blockade with CNQX, while adding ketanserin and bicuculline to block 5-HT and GABA neurotransmission. CCs were measured between stimulus trials and after stimulation. Without CNQX (n=9), CCs were not strengthened during 9-Hz synaptic stimulation (7 ± 7% increase) but significant CC strengthening was observed when stimulation was completed ($p < 0.05$; 28 ± 13% increase; Figure 7D). Repeating the experiment with CNQX (n=7) unmasked a strengthening of CCs during stimulation ($p < 0.01$; 22 ± 6% increase) which was maintained post-stimulation ($p < 0.05$; 22 ± 8% increase; Figure 7E). Adding DL-threo-β-benzyloxyaspartate (TBOA; Shimamato et al., 1998, n=6 pairs) to block glutamate reuptake (Figure 7E) broadened EPSPs (τ 29 ± 1 ms to 46 ± 3 ms with TBOA) while EPSP amplitude trended toward increase (2.8 ± 0.7 mV to 3.2 ± 0.9 mV). TBOA amplified the strengthening of CCs both during ($p < 0.01$; 33 ± 4% increase) and after stimulation ($p < 0.05$; 49 ± 18% increase). The changes in CCs with the various manipulations were not due to changes in G_{in} (Table S1). The results were consistent with an effect of synaptic NMDAR activation to strengthen coupling that only became evident after an effect of AMPAR activation to weaken coupling had subsided. The facilitating effect of TBOA was consistent both with increased availability of glutamate to synaptic

NMDARs as well as with a potential role for extrasynaptic NMDARs activated by the possible spillover of glutamate out of the synaptic cleft.

Ca^{2+} microdomains related to NMDAR-induced synchronization

The necessity of CaMKII for NMDAR-mediated strengthening of coupling implicated dendritic Ca^{2+} as an intracellular signal near GJs. To examine whether the spatial dynamics of Ca^{2+} evoked by NMDAR activation supported that hypothesis, we performed rapid 2-p Ca^{2+} imaging of electrically-coupled dendritic arbors in cell pairs filled with Fluo-4 using an array of 64 pulsed-infrared laser beams (Figure S5).

NMDAR activation increased the tonic level of intradendritic Ca^{2+} during the induction of synchronized STOs among electrically-coupled neurons (n=6 coupled neurons). Changes in fluorescence (ΔF/F) were not spatially uniform during NMDAR activation, but were especially strong (163 ± 37% increase, n=10) in bulbous swellings interspersed throughout the dendritic arbors termed “dendritic varicosities” (DVs, Figure S2), which are loci where spines extend from the dendrite to form GJs (De Zeeuw et al., 1998). The magnitude of the Ca^{2+} responses within DVs contrasted sharply with the responses of neighboring lengths of dendritic shaft which showed significantly smaller ΔF/F (79 ± 13%, n=10; $p < 0.05$) during NMDAR activation (Figure 8A). Figure 8B shows 2-p structural and Ca^{2+} activity images of dendrite segments that contained both DVs and dendritic shafts. It can be seen that DVs (green arrows) showed robust Ca^{2+} responses during NMDAR activation as compared to neighboring shafts (blue brackets). Simultaneous recordings of somatic voltage and Ca^{2+} responses throughout two neurons’ dendritic arbors (Figure 8C) demonstrated that the induction of synchronized STOs by NMDA in electrically-coupled neurons was coincident with robust increases in ΔF/F specific to DVs (Figure 8D). The imaging extended the dual-intracellular CaMKII blocking experiment by indicating an important role of Ca^{2+} signaling localized to DVs and near GJs as a mechanism by which NMDAR activation strengthens electrical coupling.

DISCUSSION

The principal finding is that electrical synapses are strengthened by NMDAR activation in the rat IO. To our knowledge, this is the first demonstration of receptor-mediated strengthening of electrical coupling in the mature mammalian brain. The finding fills a gap in our knowledge of the modifiability of electrical synaptic neurotransmission by chemical synaptic receptors. Together with known chemical synapse inhibition of electrical synapses (Landisman and Connors, 2005; Lang et al., 1996; Llinás, 1974), the mechanism we have described in which NMDAR activation strengthens electrical coupling introduces a bidirectional means of modulation.

There are three properties of NMDAR-induced strengthening of electrical coupling that determine its consequence on neuronal operations: 1) it is restricted to neurons that are weakly-coupled; 2) it upregulates coupling mainly between neurons with non-adjacent somata; 3) NMDAR activation does not strengthen coupling beyond the strength of directly adjacent neurons. Thus, NMDAR strengthening of electrical coupling does not augment the maximum gain of coupling, but rather expands the distance over which neurons are

maximally coupled. Based on those properties, the effect of NMDAR activation would be especially important within syncytia of coupled neurons in which CCs fall off rapidly with small increases in interneuronal distance. In such an arrangement, NMDAR activation decreases the electrotonic distance between neurons and increases the probability of their influencing one another.

Implications of synaptic and extrasynaptic NMDARs close to GJs

The presence of synaptic NMDARs within IO glomeruli and extrasynaptic NMDARs directly adjacent to GJs informs a new view of how glutamatergic neurotransmission may modulate the function of neuronal ensemble activity. As demonstrated here and by previous work, glutamatergic terminals (Sotelo et al., 1974; De Zeeuw et al., 1989, 1990) and NMDAR-containing PSDs (Hoge et al., 2011) can reside close (300–500 nm) to GJs, suggesting a functional interaction. Extrasynaptic NMDARs farther than 300 nm away from PSDs but as close as 20 nm to GJs suggest glutamate spillover could complement the function of synaptic NMDARs to strengthen electrical coupling. Activation of extrasynaptic NMDARs *via* glutamate spillover has been described in olfactory bulb (Isaacson, 1999) and cerebellum (Carter and Regehr, 2000) and had been hypothesized to entrain rhythmic firing (Scanziani, 2000).

Extrasynaptic NMDARs may provide an important locus for ambient glutamate to tonically regulate electrical coupling. This is supported by the finding that MK-801 abolishes spontaneous STOs in the IO that persist in the presence of other synaptic blockers and TTX (Placantonakis and Welsh, 2001). Indeed, extrasynaptic NMDARs can undergo tonic activation by ambient glutamate (Le Meur et al., 2007; Sah et al., 1989). It is estimated that ambient extracellular glutamate *in vivo* ranges from 1–4 μM (Lerma et al., 1986; Nyitrai et al., 2006). Concentrations of ambient glutamate are significant since the EC_{50} to activate NMDARs is approximately 2 μM (Patneau and Mayer, 1990). It is noteworthy that extracellular glutamate in brain slices is lower, with estimates in the nanomolar range (Cavelier and Attwell, 2005; Le Meur et al., 2007). Artificially low concentrations of extrasynaptic glutamate *ex-vivo* may be responsible for low tonic NMDAR activation and may contribute to heterogeneity in CCs among equally spaced neurons *in vitro* that may differ from a stronger and more homogeneous level of coupling *in vivo*.

An important source of ambient glutamate and non-synaptic activation of NMDARs is diffusive release of glutamate by astrocytes (Bezzi et al., 1998; Fellin et al., 2004). Although its relevance *in vivo* is debated (Nedergaard and Verkhratsky, 2012), astrocytic glutamate release could shape the activity of electrically-coupled networks in the IO since astrocytic processes are present within dendritic glomeruli (Sotelo et al., 1974; De Zeeuw et al., 1989, 1990). Because ambient glutamate is also regulated by glial uptake (Anderson and Swanson, 2000) the magnitude of NMDAR activation may be modulated by glial processes within dendritic glomeruli.

Ca^{2+} signaling and CaMKII necessity

Microdomains of increased Ca^{2+} within DVs during NMDAR activation implicated Ca^{2+} signaling in the strengthening of electrical coupling. DVs contain dendritic lamellar bodies

that reside close to electrically-coupled spines and may participate in GJ protein synthesis and assembly (De Zeeuw et al., 1995, 1998). The tonic increase in Ca^{2+} in DVs was consistent with the enhancement of G_{in} resulting from the opening of NMDAR channels. Although the increase in G_{in} would be expected to produce current shunting and thereby reduce G_j, G_j was instead increased by NMDAR activation in neurons that were weakly or moderately coupled at baseline. The enhancement of G_j and increase in CC was associated with STO synchronization. The combined enhancement in G_j and G_{in} suggested an active process in which the opening of Ca^{2+}-permeable channels enhanced G_j to a greater extent than it enhanced G_{in}. The effect of NMDAR activation to enhance G_j in weakly coupled neurons suggested that a low baseline G_j was necessary for NMDAR's effect on coupling. A low baseline G_j would be most probable for neurons having submaximal overlap of their dendritic arbors and lower probability of spine apposition. A recent calculation indicated that only 0.1% of GJ channels are conductive (Curti et al., 2012) which indicates a large pool of nonconducting channels is available for strengthening. Our paired recordings indicated that a small increase in CC from a low baseline can have a significant functional impact as evidenced by the synchronization of STOs.

Stimulation of CaMKII was necessary for NMDAR strengthening of electrical coupling as demonstrated with two mechanistically distinct inhibitors and means of delivery. Our findings were consistent with previous reports demonstrating the interaction of CaMKII with Cx36 in the central synapse of the teleost VIIIth nerve (Pereda et al., 1998), rabbit retina (Kothmann et al., 2012) and in a mouse neuroblastoma expression system (Del Corsso et al., 2012). Interestingly, CaMKII stimulation enables not only its enzymatic kinase activity, but also its direct binding to the NMDAR subunit GluN2B and to the GJ protein Cx36 (Alev et al., 2008; Coultrap and Bayer, 2012). CaMKII binding to both GluN2B and Cx36 is induced by Ca^{2+}/calmodulin (blocked by KN93) and mediated by the T-site on CaMKII (blocked by tatCN21). Thus, both binding reactions should be blocked by both CaMKII inhibitors, as was demonstrated for GluN2B binding (Vest et al., 2007; Vest et al., 2010). While our results provide evidence for the requirement of CaMKII and its stimulation, specific CaMKII protein interactions may also be required, as is the case for potentiation of glutamatergic synapses (Coultrap and Bayer, 2012). The 12meric holoenzyme structure of CaMKII allows multi-valent interactions with several proteins, which could theoretically include CaMKII-mediated crosslinking of NMDARs with Cx36-containing GJs. However, this is likely not part of the novel mechanism elucidated here, based on the size of the CaMKII holoenzyme (~20 nm diameter) and the distance observed between extrasynaptic NMDARs and GJs (20–100 nm).

Roles for strengthened electrical coupling

It is known that STOs of IO neurons are expressed *in vivo* where they entrain action potentials (Bazzigaluppi et al., 2012a; Chorev et al., 2007; Khosrovani et al., 2007) and that the strength and synchrony of STOs is supported by electrical coupling (Long et al., 2002; Placantonakis et al., 2006, Van der Giessen et al., 2008). Reconfigurations of the spatial patterning of IO synchrony recur during movement and implicated synaptic control in the structure of an underlying continuous oscillator (Welsh et al., 1995).

One role for NMDAR strengthening of electrical coupling may be to establish a baseline level of coupling sufficient to permit continuous STOs to emerge within a system comprised of weakly-coupled, non-continuous oscillators. G_j between IO neurons is only 50–200 pS (Figure S4) which is remarkably weak compared to the G_j in other systems, such as retina AII amacrine cells (400 pS; Veruki et al., 2010), mesencephalic trigeminal neurons (4.8 nS; Curti et al., 2012), and crayfish septate axons (10 μS; Campos de Carvalho et al., 1984). A tonic NMDAR current mediating Ca^{2+} influx at DVs and GJs may increase G_j between weaklycoupled neurons to a level sufficient to permit continuous STOs to emerge within an ensemble.

A second role may be to broaden the area over which groups of neurons can spike synchronously as a consequence of synchronizing STOs. Because G_j between IO neurons is weak and acts as a low-pass filter, coupling does not allow a spike in one neuron to trigger a spike in a coupled neuron (Llinás et al., 1974). Because weak electrical coupling is prevalent in the IO, its strengthening suggests that glutamate may elevate coupling strength to a level sufficient to synchronize STOs but below the level required to conduct spikes across the GJ. Expanding the size of the coupled network by NMDAR activation provides a mechanism for dynamically regulating the size of the population whose STOs are synchronized and thereby more likely to spike synchronously.

A third role for strengthening electrical coupling may be to counterbalance the decrease in coupling produced by co-activation of other ionotropic glutamate receptors. Depolarizing the post-junctional membrane with direct current decreased coupled potentials (Devor and Yarom, 2002) consistent with an influence of current shunt during membrane rectification. Our experiments demonstrated AMPAR-mediated shunting with pharmacological activation and demonstrated that its inhibitory influence is restricted to the duration of synaptic activation. Thus, in the presence of strong excitatory input in which increased G_{in} due to AMPAR activation shunts current away from GJs, co-activation of synaptic NMDARs and possibly glutamate spillover to extrasynaptic NMDARs adjacent to GJs may thereafter prolong STO synchrony by strengthening G_j beyond the duration of the shunt.

General implications

NMDAR expression is prevalent in mammalian brain systems that contain neurons that are electrically coupled and where the consequence of NMDAR activation is oscillation and synchrony. For example, NMDARs are expressed in electrically-coupled, parvalbuminexpressing inhibitory interneurons in cerebral cortex where their activation induces synchronous firing and is necessary for spontaneous and induced gamma oscillations (Carlén et al., 2012; Korotkova et al., 2010). The enhancement of GJ conductances by NMDARs may be conserved and may generalize. Indeed, the conductance mediated by hemi-channels comprised of pannexin proteins – the mammalian homolog of the innexin insect GJ proteins (Yen and Saier, 2007) – also is potentiated by NMDAR activation and has been implicated in anoxic depolarization and neuron death after ischemia (Weilinger et al., 2012). Similarly, mammalian GJs comprised of Cx36 are required for NMDAR-mediated excitotoxicity (Wang et al., 2010). Based on the above, NMDAR

strengthening of weak electrical synapses may be significant for normal and pathological functions in mammalian brain.

EXPERIMENTAL PROCEDURES

Light microscopy

GFP was expressed in the IO of Sprague-Dawley rats (250 g) by stereotaxic injection of recombinant lentivirus. The IO was immunolabeled for the presence of NR1 and Cx36 within GFP-expressing dendrites and imaged with a confocal microscope (Figure S1).

Electronmicroscopy

Sections were immersed in 25% sucrose and 3% glycerol in 0.05 M PB (15 min) then immersed in Freon followed by liquid nitrogen (method of S. Aicher assisting G.S.Y.). Sections were treated with mouse anti-NR1 antisera (1:10; Chemicon). NR1 was visualized by immunogold labeling using goat anti-mouse IgG conjugated to 1 nm colloidal gold (1:50, Amersham). Incubations contained 0.1% BSA at 22° C (1 h) followed by 4° C (4 h). Sections were rinsed in citrate buffer. Colloidal gold was enhanced by silver intensification (IntenSEM, Amersham, Piscataway, NJ). Sections were fixed in 2% osmium tetroxide in 0.1 M PB (1 h), washed (0.1 M PB, 10 min), dehydrated using an ethanol series followed by propylene oxide and propylene oxide:EMBed (Electronmicroscopy Sciences, Fort Washington, PA; 1:1) solution, incubated in EMBed (2 h), embedded between Aclar sheets (60° C, 1–2 d), and glued to plastic blocks; 75 nm sections were collected onto copper grids and counterstained with uranyl acetate and Reynolds lead citrate. Images from the medial accessory olive were obtained using a Philips 201 electronmicroscope, recorded to 3.75×3.25 in film, and digitized (2400 pixels/in).

Electrophysiology

Rat brainstems (P24-P50) were cut parasagittaly (250 μm) in chilled sucrose ACSF made from (mM): sucrose 252, KCl 5, $NaH_2PO_4•H_2O$ 1.25, $NaHCO_3$ 26, $CaCl_2•2H_2O$ 0.5, $MgSO_4•7H_2O$ 3.5, glucose 10, oxygenated with 95% O_2/5% CO_2 to pH 7.4 (305–315 mOsm). Slices were incubated in the solution (1 h) which was replaced with ACSF containing (mM): NaCl 126, KCl 5, $NaH_2PO_4•H_2O$ 1.25, $NaHCO_3$ 26, $CaCl_2•2H_2O$ 2, $MgSO_4•7H_2O$ 2, glucose 10 and oxygenated with 95% O_2/5% CO_2 to pH 7.4 for at least 1 h prior to recording (2–3 ml/min, 32° C, Hoge et al., 2011, allowing greater than 50% neurons with intrinsic STOs; Olympus BX-51WI microscope). Electrodes (3–6 MΩ) were filled with a solution of (mM): K gluconate 130, EGTA 5, HEPES 10, KCl 5, $CaCl_2•H_2O$ 0.5, $MgSO_4•7H_2O$ 2, Na2ATP 4, Na_2phosphocreatine 5, Na_3GTP 0.3. A Multiclamp 700B amplifier and Digidata 1440A (Molecular Devices) were used.

Electrical coupling was quantified by injecting hyperpolarizing current into one of 2 neurons during dual recording, measuring both voltage responses, and calculating their ratio to derive the CC (Bennett, 1966; Devor and Yarom, 2002). Hyperpolarizing current injections (1 s intervals) were 200 ms and −300 or −500 pA. Averages (30–50 trials) were used to calculate CCs which were measured from the average voltage 100 ms before current offset to minimize contribution of capacitive coupling. Drug effects were assessed beginning at 7

min. CCs were determined only for neurons that had a stable membrane potential. Gj was calculated as: $G_j = 1/[[(R_{in}$ cell 1)*(R_{in} cell 2)–(transfer resistance)^2]/transfer resistance] (Bennett, 1966). Transfer resistance was defined as the voltage response in cell 2 when current was injected into cell 1 divided by the amplitude of the current step. STOs were periodic waveforms with mean amplitude exceeding 0.3 mV. Synaptic activation experiments stimulated the RF at least 100 μm from the IO (PPS or 400–500 ms trains of 9 or 50 Hz stimuli, every 2–3 s for 3–4 min, tungsten bipolar electrode, 100–300 μA *via* a constant current stimulator adjusted below spike threshold). Stimulation did not occur before measuring CCs. NMDAR isolation was conducted in 0 Mg^{2+} ACSF, bicuculline, ketanserin, and CNQX, during $NiCl_2$ and CsCl to block STOs, and TBOA as needed and was confirmed by subtracting stimulation under AP5 after each experiment.

Rapid 2-p imaging

Fluo-4 (100 μM) was added to the electrode solution. Imaging used 64 pulsed-infrared laser beams (810 nm) to excite dendritic arbors at 20–40 Hz (Figure S5). Structural images were obtained with a photomultiplier tube and single beam scanning. Rapid imaging was conducted at the z-plane with the largest area of dendritic overlap between recorded pairs. NMDA was applied for 10 min during imaging and dual recordings. Multiple regions of interest were selected and brightness was measured offline (ImageJ, NIH).

Tracer coupling

Neurobiotin (0.5%) was iontophoretically injected (0.2 Hz, 250 ms, 500 pA pulses, 10 min) while tissue was bathed in normal ACSF or ACSF with 30 μM NMDA. After the electrode was removed the slice was incubated in the same solution (25° C, 60–80 min), fixed overnight (4° C) in 4% paraformaldehyde in 0.1 M PB, washed 3 times (0.1 M PB, pH 7.4, 10 min), once in PB containing 0.5% Triton, and incubated with Alexa Fluor 568-conjugated streptavidin (3 h, 7.5 mg/ml, Invitrogen) and 0.25% Triton in 0.1M PB. Confocal images (20–50 z-sections, 1–2 μm spacing) were obtained (fixed laser intensity, gain adjusted to visualize all tracer-coupled cells) and analyzed (ImageJ) to measure somata position and brightness. The mean and standard deviation of the background brightness was recorded for a 40×40 μm region without labeling. Somata less than 1 standard deviation of background were excluded. Only “curly” neurons were analyzed (Devor and Yarom, 2002).

Drugs

Drugs (Sigma, μM) were AP5 (100), AMPA (10), bicuculline (10), CsCl (2 mM), KA (20), ketanserin (1), KN-93 (1), MK-801 (50), $NiCl_2$ (50), nifedipine (50–75), NMDA (30 or 50), tatCN21 and tatCtrl (15, synthesized by K.U.B.), and TBOA (100, Tocris). Drugs were dissolved in ACSF (0.001% DMSO as needed) and tatCN21 and tatCtrl were dissolved in water before into the internal electrode solution.

Statistics

Completely randomized and mixed analyses of variance (ANOVA) were used. *Post-hoc* analyses used Fisher’s LSD test to control for multiple comparisons. Fisher’s Exact test was used to determine differences in the proportion of cells showing electrical coupling. T-tests

were used for comparisons of tracer coupling and changes in ΔF/F. Significance was $p < 0.05$. Data are presented as the mean ± 1 standard error of the mean (SEM). Animal procedures were approved by Cornell and Seattle Children's Animal Use Committees.

Supplementary Material

Refer to Web version on PubMed Central for supplementary material.

ACKNOWLEDGMENTS

Supported by NIH Grant R01 NS31224-19, the Myoclonus Research Foundation (J.P.W), the Mary Gates Foundation (J.T.) and NIH Grant R01 NS081248 (K.U.B.). J.T., G.Y., V.Z.H., X.H.Z., J.P.W. performed experiments. K.U.B. provided input on CaMKII signaling and inhibition. J.T. and J.P.W. designed experiments, analyzed data, wrote the paper.

REFERENCES

Alev C, Urschel S, Sonntag S, Zoidl G, Fort AG, Höher T, Matsubara M, Willecke K, Spray DC, Dermietzel R. The neuronal connexin36 interacts with and is phosphorylated by CaMKII in a way similar to CaMKII interaction with glutamate receptors. Proc. Natl. Acad. Sci. USA. 2008; 105:20964–20969. [PubMed: 19095792]

Anderson CM, Swanson RA. Astrocyte glutamate transport: review of properties, regulation, and physiological functions. Glia. 2000; 32:1–14. [PubMed: 10975906]

Bazzigaluppi P, Ruigrok T, Saisan P, De Zeeuw CI, de Jeu M. Properties of the nucleo-olivary pathway: an in vivo whole-cell patch clamp study. PLoS One. 2012a; 7:e46360. [PubMed: 23029495]

Bazzigaluppi P, De Gruijl JR, Van Der Giessen RS, Khosrovani S, De Zeeuw CI, de Jeu MT. Olivary subthreshold oscillations and burst activity revisited. Front. Neural Circuits. 2012b; 6:91. [PubMed: 23189043]

Bennett MV. Physiology of electrotonic junctions. Ann. NY Acad. Sci. 1966; 137:509–539. [PubMed: 5229812]

Best AR, Regehr WG. Inhibitory regulation of electrically coupled neurons in the inferior olive is mediated by asynchronous release of GABA. Neuron. 2009; 62:555–565. [PubMed: 19477156]

Bezzi P, Carmignoto G, Pasti L, Vesce S, Rossi D, Rizzini BL, Pozzan T, Volterra A. Prostaglandins stimulate calcium-dependent glutamate release in astrocytes. Nature. 1998; 391:281–285. [PubMed: 9440691]

Campos de Carvalho A, Spray DC, Bennett MV. pH dependence of transmission at electrotonic synapses of the crayfish septate axon. Brain Res. 1984; 321:279–286. [PubMed: 6093934]

Carew TJ, Kandel ER. Two functional effects of decreased conductance EPSP's: synaptic augmentation and increased electrotonic coupling. Science. 1976; 192:150–153. [PubMed: 943847]

Carlén M, Meletis K, Siegle JH, Cardin JA, Futai K, Vierling-Claassen D, Rühlmann C, Jones SR, Deisseroth K, Sheng M, Moore CI, Tsai LH. A critical role for NMDA receptors in parvalbumin interneurons for gamma rhythm induction and behavior. Mol. Psychiatry. 2012; 17:537–548. [PubMed: 21468034]

Carter AG, Regehr WG. Prolonged synaptic currents and glutamate spillover at the parallel fiber to stellate cell synapse. J. Neurosci. 2000; 20:4423–4434. [PubMed: 10844011]

Cavelier P, Attwell D. Tonic release of glutamate by a DIDS-sensitive mechanism in rat hippocampal slices. J. Physiol. 2005; 564:397–410. [PubMed: 15695241]

Chorev E, Yarom Y, Lampl I. Rhythmic episodes of subthreshold membrane potential oscillations in the rat inferior olive nuclei in vivo. J. Neurosci. 2007; 27:5043–5052. [PubMed: 17494690]

Condorelli DF, Parenti R, Spinella F, Trovato Salinaro A, Belluardo N, Cardile V, Cicirata F. Cloning of a new gap junction gene (Cx36) highly expressed in mammalian brain neurons. Eur. J. Neurosci. 1998; 10:1202–1208. [PubMed: 9753189]

Coultrap SJ, Bayer KU. CaMKII regulation in information processing and storage. Trends Neurosci. 2012; 35:607–618. [PubMed: 22717267]

Curti S, Hoge G, Nagy JI, Pereda AE. Electrical transmission between mammalian neurons is supported by a small fraction of gap junction channels. J. Membr. Biol. 2012; 245:283–290. [PubMed: 22729690]

De Gruijl JR, Bazzigaluppi P, de Jeu MTG, De Zeeuw CI. Climbing fiber burst size and olivary sub-threshold oscillations in a network setting. PLOS Comp. Biol. 2012; 8:e1002814.

Devor A, Yarom Y. Electrotonic coupling in the inferior olivary nucleus revealed by simultaneous double patch recordings. J. Neurophysiol. 2002; 87:3048–3058. [PubMed: 12037207]

De Zeeuw CI, Chorev E, Devor A, Manor Y, Van der Giessen RS, de Jeu MT, Hoogenraad CC, Bijman J, Ruigrok TJ, French P, Jaarsma D, Kistler WM, Meier C, Petrasch-Parwez E, Dermietzel R, Sohl G, Gueldenagel M, Willecke K, Yarom Y. Deformation of network connectivity in the inferior olive of connexin 36-deficient mice is compensated by morphological and electrophysiological changes at the single neuron level. J. Neurosci. 2003; 23:4700–4711. [PubMed: 12805309]

De Zeeuw CI, Hertzberg EL, Mugnaini E. The dendritic lamellar body: a new neuronal organelle putatively associated with dendrodendritic gap junctions. J. Neurosci. 1995; 15:1587–1604. [PubMed: 7869120]

De Zeeuw CI, Holstege JC, Ruigrok TJH, Voogd J. Ultrastructural study of the GABAergic, cerebellar, and mesodiencephalic innervation of the cat medial accessory olive: anterograde tracing combined with immunocytochemistry. J. Comp. Neurol. 1989; 284:12–35. [PubMed: 2474000]

De Zeeuw CI, Holstege JC, Ruigrok TJ, Voogd J. Mesodiencephalic and cerebellar terminals terminate upon the same dendritic spines in the glomeruli of the cat and rat inferior olive: an ultrastructural study using a combination of [3H]leucine and wheat germ agglutinin coupled horseradish peroxidase anterograde tracing. Neuroscience. 1990; 34:645–655. [PubMed: 1693761]

De Zeeuw CI, Simpson JI, Hoogenraad CC, Galjart N, Koekkoek SK, Ruigrok TJ. Microcircuitry and function of the inferior olive. Trends Neurosci. 1998; 21:391–400. [PubMed: 9735947]

Del Corsso C, Iglesias R, Zoidl G, Dermietzel R, Spray DC. Calmodulin dependent protein kinase increases conductance at gap junctions formed by the neuronal gap junction protein connexin36. Brain Res. 2012; 1487:69–77. [PubMed: 22796294]

Enslen H, Sun P, Brickey D, Soderling SH, Klamo E, Soderling TR. Characterization of Ca2+/calmodulin-dependent protein kinase IV. Role in transcriptional regulation. J. Biol. Chem. 1994; 269:15520–15527. [PubMed: 8195196]

Fellin T, Pascual O, Gobbo S, Pozzan T, Haydon PG, Carmignoto G. Neuronal synchrony mediated by astrocytic glutamate through activation of extrasynaptic NMDA receptors. Neuron. 2004; 43:729–743. [PubMed: 15339653]

Gao L, Blair LA, Marshall J. CaMKII-independent effects of KN93 and its inactive analog KN92: reversible inhibition of L-type calcium channels. Biochem. Biophys. Res. Comm. 2006; 345:1606–1610. [PubMed: 16730662]

Hoge GJ, Davidson KG, Yasumura T, Castillo PE, Rash JE, Pereda AE. The extent and strength of electrical coupling between inferior olivary neurons is heterogeneous. J. Neurophysiol. 2011; 105:1089–1101. [PubMed: 21177999]

Khosrovani S, Van der Giessen RS, De Zeeuw CI, de Jeu MT. In vivo mouse inferior olive neurons exhibit heterogeneous subthreshold oscillations and spiking patterns. Proc. Natl. Acad. Sci. USA. 2007; 104:15911–15916. [PubMed: 17895389]

Korotkova T, Fuchs EC, Ponomarenko A, von Engelhardt J, Monyer H. NMDA receptor ablation on parvalbumin-positive interneurons impairs hippocampal synchrony, spatial representations, and working memory. Neuron. 2010; 68:557–569. [PubMed: 21040854]

Kothmann WW, Trexler EB, Whitaker CM, Li W, Massey SC, O'Brien J. Nonsynaptic NMDA receptors mediate activity-dependent plasticity of gap junctional coupling in the AII amacrine cell network. J. Neurosci. 2012; 32:6747–6759. [PubMed: 22593045]

Isaacson JS. Glutamate spillover mediates excitatory transmission in the rat olfactory bulb. Neuron. 1999; 23:377–384. [PubMed: 10399942]

Landisman CE, Connors BW. Long-term modulation of electrical synapses in the mammalian thalamus. Science. 2005; 310:1809–1813. [PubMed: 16357260]

Lang EJ, Sugihara I, Llinás R. GABAergic modulation of complex spike activity by the cerebellar nucleoolivary pathway in rat. J. Neurophysiol. 1996; 76:255–275. [PubMed: 8836223]

Ledoux J, Chartier D, Leblanc N. Inhibitors of calmodulin-dependent protein kinase are nonspecific blockers of voltage-dependent K+ channels in vascular myocytes. J. Pharmacol. Exp. Ther. 1999; 290:1165–1174. [PubMed: 10454491]

Le Meur K, Galante M, Angulo MC, Audinat E. Tonic activation of NMDA receptors by ambient glutamate of non-synaptic origin in the rat hippocampus. J. Physiol. 2007; 580:373–383. [PubMed: 17185337]

Lerma J, Herranz AS, Herreras O, Abraira V, Del Rio RM. In vivo determination of extracellular concentration of amino acids in the rat hippocampus. A method based on brain dialysis and computerized analysis. Brain Res. 1986; 384:145–155. [PubMed: 3790989]

Llinás R, Baker R, Sotelo C. Electrotonic coupling between neurons in cat inferior olive. J. Neurophysiol. 1974; 37:560–571. [PubMed: 4827022]

Llinás R, Sasaki K. The functional organization of the olivo-cerebellar system as examined by multiple Purkinje cell recordings. Eur. J. Neurosci. 1989; 1:587–602. [PubMed: 12106117]

Long MA, Deans MR, Paul DL, Connors BW. Rhythmicity without synchrony in the electrically uncoupled inferior olive. J. Neurosci. 2002; 22:10898–10905. [PubMed: 12486184]

Nedergaard M, Verkhratsky A. Artifact versus reality-How astrocytes contribute to synaptic events. Glia. 2012; 60:1013–1023. [PubMed: 22228580]

Nyitrai G, Kekesi KA, Juhasz G. Extracellular level of GABA and Glu: in vivo microdialysis-HPLC measurements. Curr. Top. Med. Chem. 2006; 6:935–940. [PubMed: 16787267]

Patneau DK, Mayer ML. Structure-activity relationships for amino acid transmitter candidates acting at N-methyl-D-aspartate and quisqualate receptors. J. Neurosci. 1990; 10:2385–2399. [PubMed: 2165523]

Pereda AI, Bell TD, Chang BH, Czernik AJ, Nairn AC, Soderling TR, Faber DS. Ca^{2+}/calmodulin-dependent kinase II mediates simultaneous enhancement of gap-junctional conductance and glutamatergic transmission. Proc. Natl. Acad. Sci. USA. 1998; 95:13272–13277. [PubMed: 9789078]

Pereda AI, Faber DS. Activity-dependent short-term enhancement of intercellular coupling. J. Neurosci. 1996; 16:983–992. [PubMed: 8558267]

Placantonakis DG, Bukovsky AA, Aicher SA, Kiem HP, Welsh JP. Continuous electrical oscillations emerge from a coupled network: a study of the inferior olive using lentiviral knockdown of connexin36. J. Neurosci. 2006; 26:5008–5016. [PubMed: 16687492]

Placantonakis D, Welsh JP. Two distinct oscillatory states determined by the NMDA receptor in rat inferior olive. J. Physiol. 2001; 534:123–140. [PubMed: 11432997]

Petralia RS, Wang YX, Hua F, Yi Z, Zhou A, Ge L, Stephenson FA, Wenthold RJ. Organization of NMDA receptors at extrasynaptic locations. Neuroscience. 2010; 167:68–87. [PubMed: 20096331]

Sah P, Hestrin S, Nicoll RA. Tonic activation of NMDA receptors by ambient glutamate enhances excitability of neurons. Science. 1989; 246:815–818. [PubMed: 2573153]

Scanziani M. GABA spillover activates postsynaptic $GABA_B$ receptors to control rhythmic hippocampal activity. Neuron. 2000; 25:673–681. [PubMed: 10774734]

Shimamoto K, Lebrun B, Yasuda-Kamatani Y, Sakaitani M, Shigeri Y, Yumoto N, Nakajima T. DL-threo-beta-benzyloxyaspartate, a potent blocker of excitatory amino acid transporters. Mol. Pharmacol. 1998; 53:195–201. [PubMed: 9463476]

Sotelo C, Llinás R, Baker R. Structural study of inferior olivary nucleus of the cat: morphological correlates of electrotonic coupling. J. Neurophysiol. 1974; 37:541–559. [PubMed: 4827021]

Spira ME, Bennett MV. Synaptic control of electrotonic coupling between neurons. Brain Res. 1972; 37:294–300. [PubMed: 4334355]

Van der Giessen RS, Koekkoek SK, van Dorp S, De Gruijl JR, Cupido A, Khosrovani S, Dortland B, Wellershaus K, Degen J, Deuchars J, Fuchs EC, Monyer H, Willecke K, De Jeu MT, De Zeeuw

CI. Role of olivary electrical coupling in cerebellar motor learning. Neuron. 2008; 58:599–612. [PubMed: 18498740]

Veruki ML, Oltedal L, Hartveit E. Electrical coupling and passive membrane properties of AII amacrine cells. J. Neurophysiol. 2010; 103:1456–1466. [PubMed: 20089813]

Vest RS, Davies KD, O'Leary H, Port JD, Bayer KU. Dual mechanism of a natural CaMKII inhibitor. Mol. Biol. Cell. 2007; 18:5024–5033. [PubMed: 17942605]

Vest RS, O'Leary H, Coultrap SJ, Kindy MS, Bayer KU. Effective postinsult neuroprotection by a novel Ca(2+)/calmodulin-dependent protein kinase II (CaMKII) inhibitor. J. Biol. Chem. 2010; 285:20675–20682. [PubMed: 20424167]

Wang Y, Denisova JV, Kang KS, Fontes JD, Zhu BT, Belousov AB. Neuronal gap junctions are required for NMDA receptor-mediated excitotoxicity: implications in ischemic stroke. J. Neurophysiol. 2010; 104:3551–3556. [PubMed: 20943940]

Weilinger NL, Tang PL, Thompson RJ. Anoxia-induced NMDA receptor activation opens pannexin channels via Src family kinases. J. Neurosci. 2012; 32:12579–12588. [PubMed: 22956847]

Welsh JP, Lang EJ, Sugihara I, Llinás R. Dynamic organization of motor control within the olivocerebellar system. Nature. 1995; 374:453–457. [PubMed: 7700354]

Yen MR, Saier MH Jr. Gap junctional proteins of animals: the innexin/pannexin superfamily. Prog. Biophys. Mol. Biol. 2007; 94:5–14. [PubMed: 17507077]

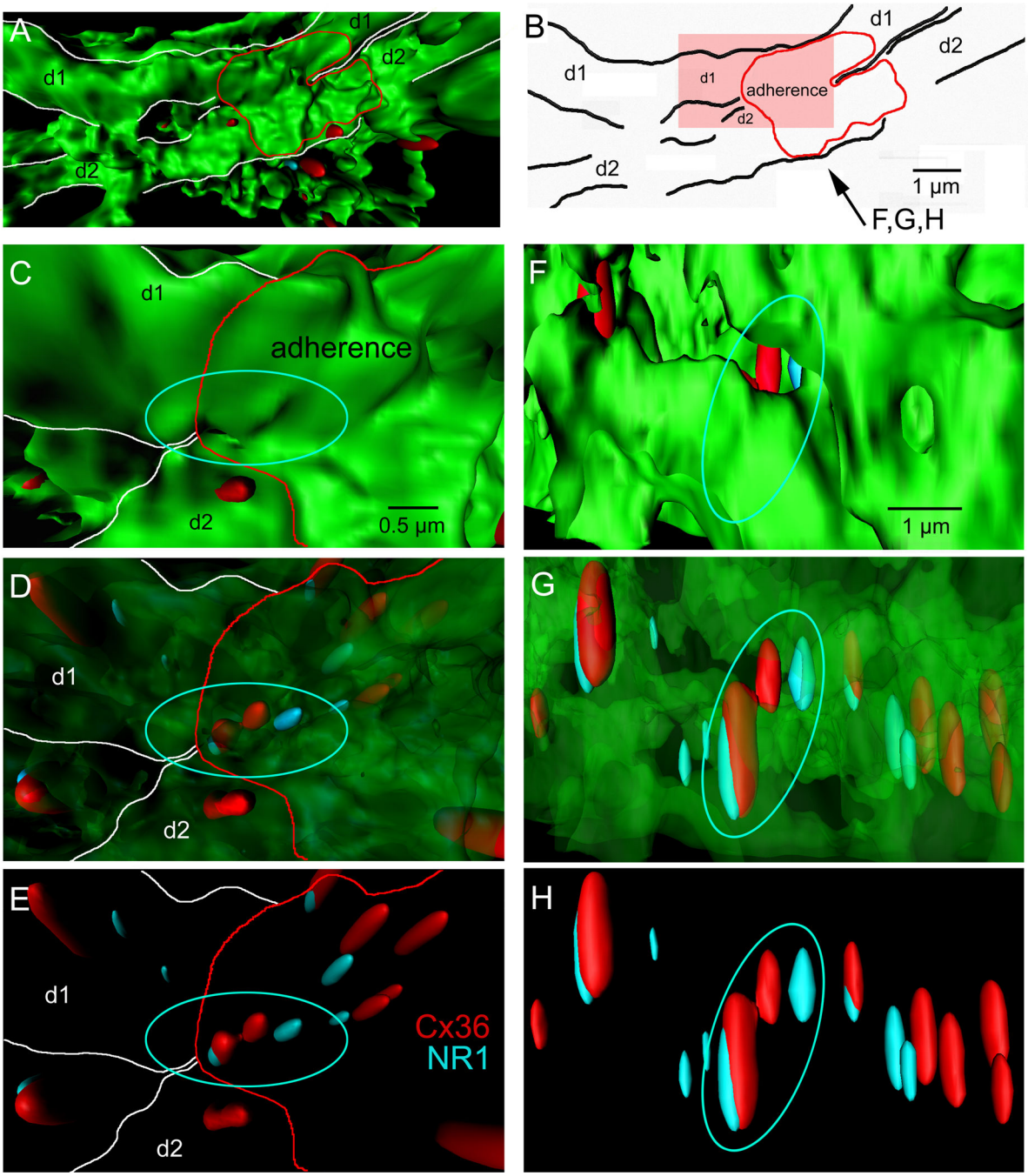

Figure 1. 3-dimensional organization of NMDA-NR1 and Cx36 in IO dendrites

(A) Surface render (top view) of 2 GFP-labeled IO dendrites (d1, d2) converging to a point of adherence (red). (B) Outline of structures shown in A. (C–E) High magnification image of the dendritic adherence (pink region in B) viewed from the top in which the GFP is progressively ghosted to reveal Cx36 (red) and NR1 (blue) immunosignals, including a quadruple-assembly of contiguous Cx36 and NR1 signals (circle) within the adherence and unassembled Cx36-NR1 pairs (arrows). (F–H) Similar displays of the same region as in C-E

from the side showing the spacing of Cx36 and NR1 within the assembly and unassembled Cx36-NR1 pairs. See also Figure S1.

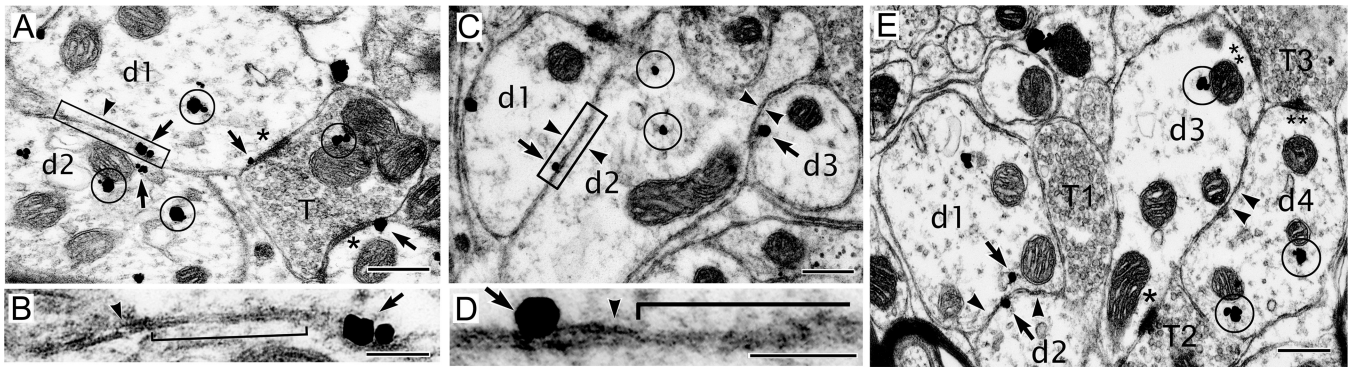

Figure 2. Synaptic and extrasynaptic NR1 within glomeruli of coupled IO dendrites

(A,B) Chemical synaptic NR1 along the margin of asymmetric PSDs (arrows next to asterisks) of IO dendrites (d) that receive an axonal terminal (T) within a glomerulus. One of the dendrites (d1) is coupled by a GJ (box in A) to another dendrite (d2) and expresses an extrasynaptic NR1 (arrow) on the apposed membrane. Both dendrites express NR1 in their cytosol (circles). (B) High magnification of box in (A) showing membrane apposition (arrowhead) and GJ (bracket) next to an extrasynaptic NR1 (arrow). (C) 3 spines coupled in series (arrowheads) express NR1 along apposed membranes (arrows). (D) High magnification of box in (C) showing NR1 expression (arrow) closely associated with membrane apposition (arrowhead) and GJ (bracket). (E) A third glomerulus showing 4 dendritic spines separated by a synaptic terminal (T1). All spines express NR1. D1 expresses an extrasynaptic NR1 along its apposition with D2, which expresses an NR1 within 50 nm of the apposition. One asterisk indicates asymmetric PSD suggesting excitatory innervation of D3 by T2; 2 asterisks indicate symmetric PSDs suggesting GABAergic innervation of D3 and D4 by T3. Scale, 250 nm (A,C,E), 100 nm (B,D).

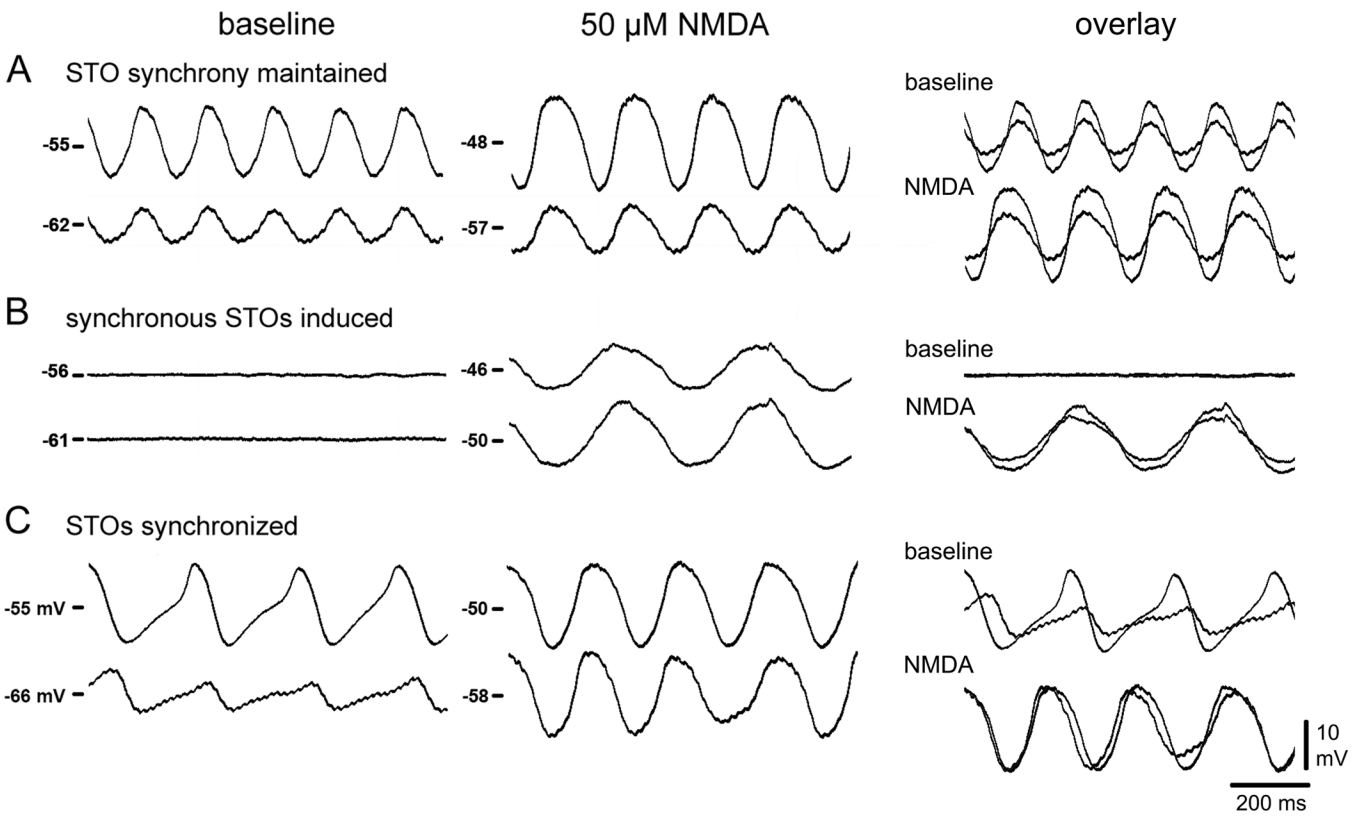

Figure 3. NMDAR activation synchronizes STOs

In 42 pairs of somata spaced < 100 μm, NMDAR activation (A) enhanced STO amplitude while maintaining synchrony; (B) induced synchronized STOs in quiescent neurons; (C) synchronized STOs that were previously asynchronous. See also Figure S2.

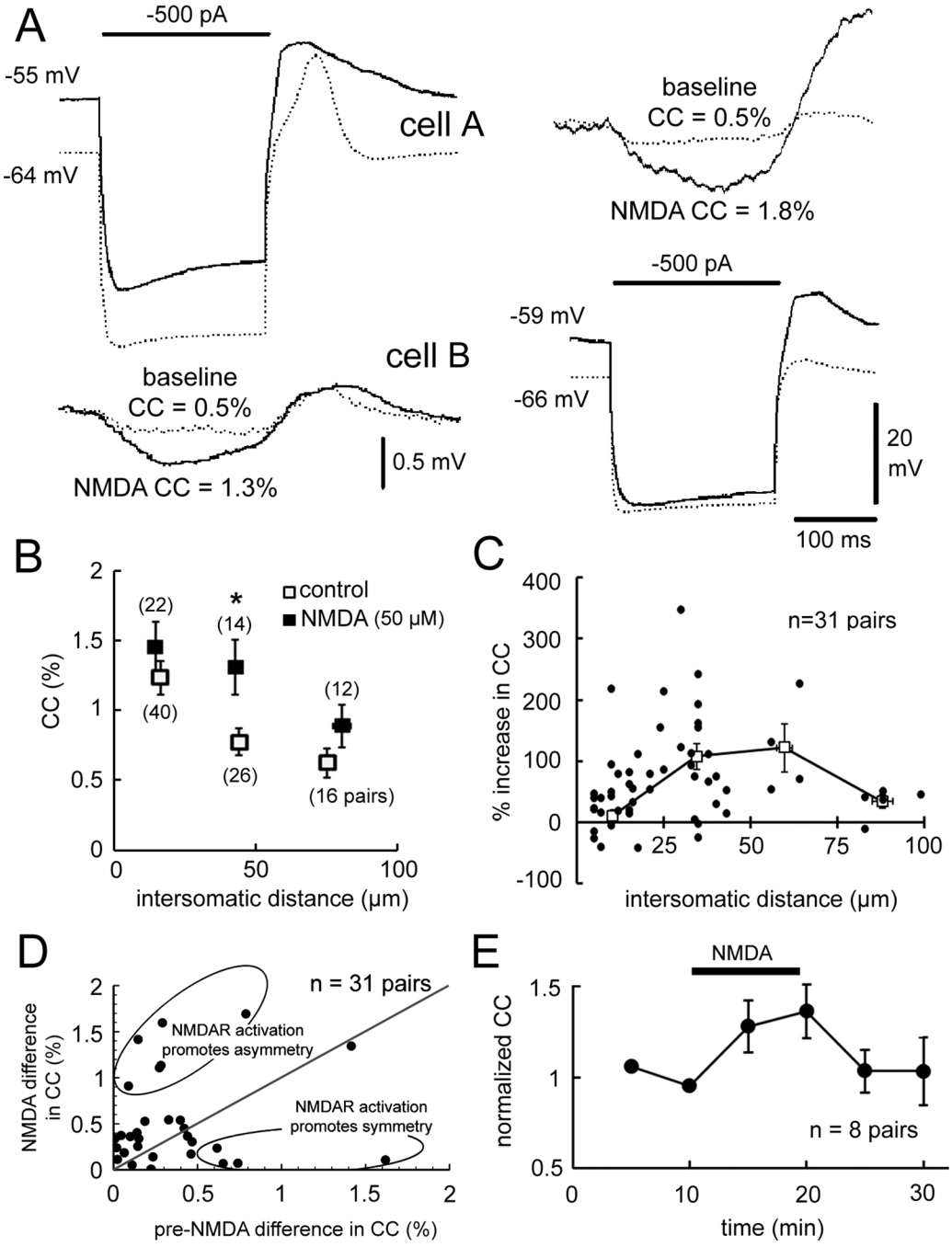

Figure 4. NMDAR activation strengthens electrical coupling

(A) Current injection into cell A or B produced coupled potentials in the simultaneously recorded neuron pre-NMDA (dotted traces) and larger coupled potentials during NMDA (solid traces). (B) CC as a function of intersomatic distance pre-NMDA and during NMDA ($p < 0.05$, 2-way ANOVA, mean ± 1 SEM). (C) Percentage change in CC by NMDA as a function of intersomatic distance. Each dot indicates a CC measurement; the curve plots mean ± 1 SEM. (D) Effect of NMDAR activation to modulate coupling asymmetry in some

cell pairs (ellipses). (E) Time course of CC strengthening by NMDAR activation ($p < 0.01$, repeated measures ANOVA, mean ± 1 SEM). See also Figure S3.

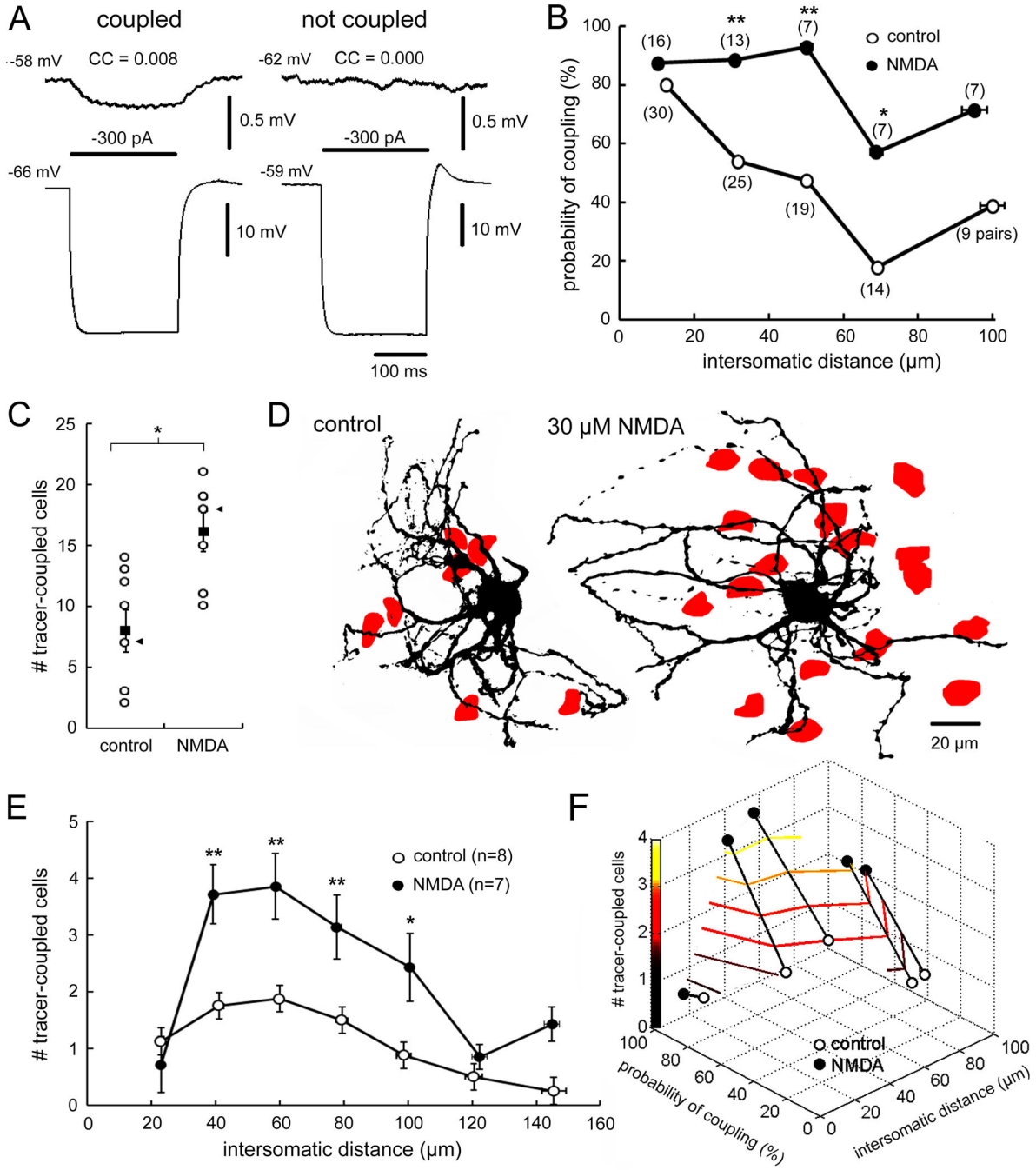

Figure 5. NMDAR activation expands electrical- and tracer-coupling

(A) Presence and absence of electrical coupling. (B) Electrical coupling probability as a function of intersomatic distance for normal ACSF and NMDA-treated neuron pairs (* $p <$ 0.05, ** $p < 0.01$, Fisher Exact test). (C) Mean ± 1 SEM (solid squares) number of tracer-coupled neurons during normal ACSF and during NMDAR activation. Cases are shown in open circles (* $p < 0.05$, t-test). (D) Tracer-coupled cells (red) within the dendritic arbors of IO neurons injected during normal ACSF and during NMDA. Cases indicated by arrowheads in (C). (E) Mean (± 1 SEM) number of tracer-coupled cells as function of

distance from the injected soma for control and NMDA-treated slices (* $p < 0.05$, ** $p < 0.01$; 2-way ANOVA and Fisher's LSD test). (F) Plot showing the relationship between number of tracer-coupled cells and probability of electrically-coupled cells over intersomatic distance and modulation by NMDA.

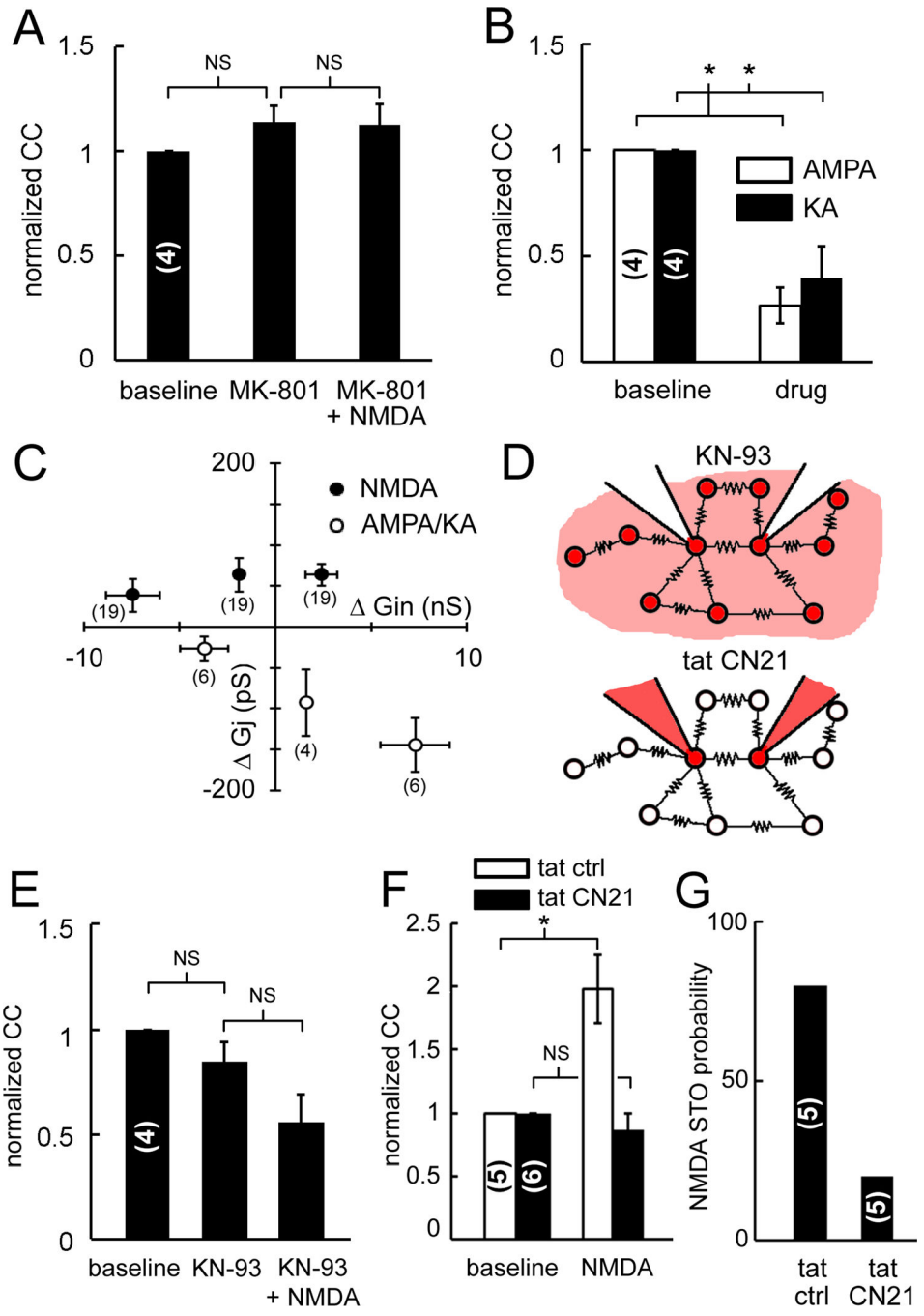

Figure 6. Receptor specificity and dependence on CaMKII activation

(A) MK801 blocks NMDAR strengthening of electrical coupling. (B) AMPA and KA nearly abolish electrical coupling. (C) NMDA enhances G_j of weakly coupled pairs as it increases G_{in} (filled symbols) while AMPA and KA reduce G_j as it increases G_{in} (open symbols). See also Figure S4. (D) CaMKII blockade used bath-applied KN-93 (top) and dual intracellular tatCN21 (bottom). (E) KN-93 did not affect baseline coupling but blocked NMDAR strengthening of coupling. (F) Intracellular tatCN21 but not tatCtrl blocked NMDAR strengthening of coupling (* $p < 0.05$, 1-way ANOVA and Fisher's LSD test). (G) STOs

during NMDA are less probable during dual intracellular tatCN21 than during intracellular tatCtrl in pairs not showing intrinsic STOs before NMDA. Parentheses indicate number of pairs (A,B,E,F,G) and direction measurements (C). All data mean ± 1 SEM.

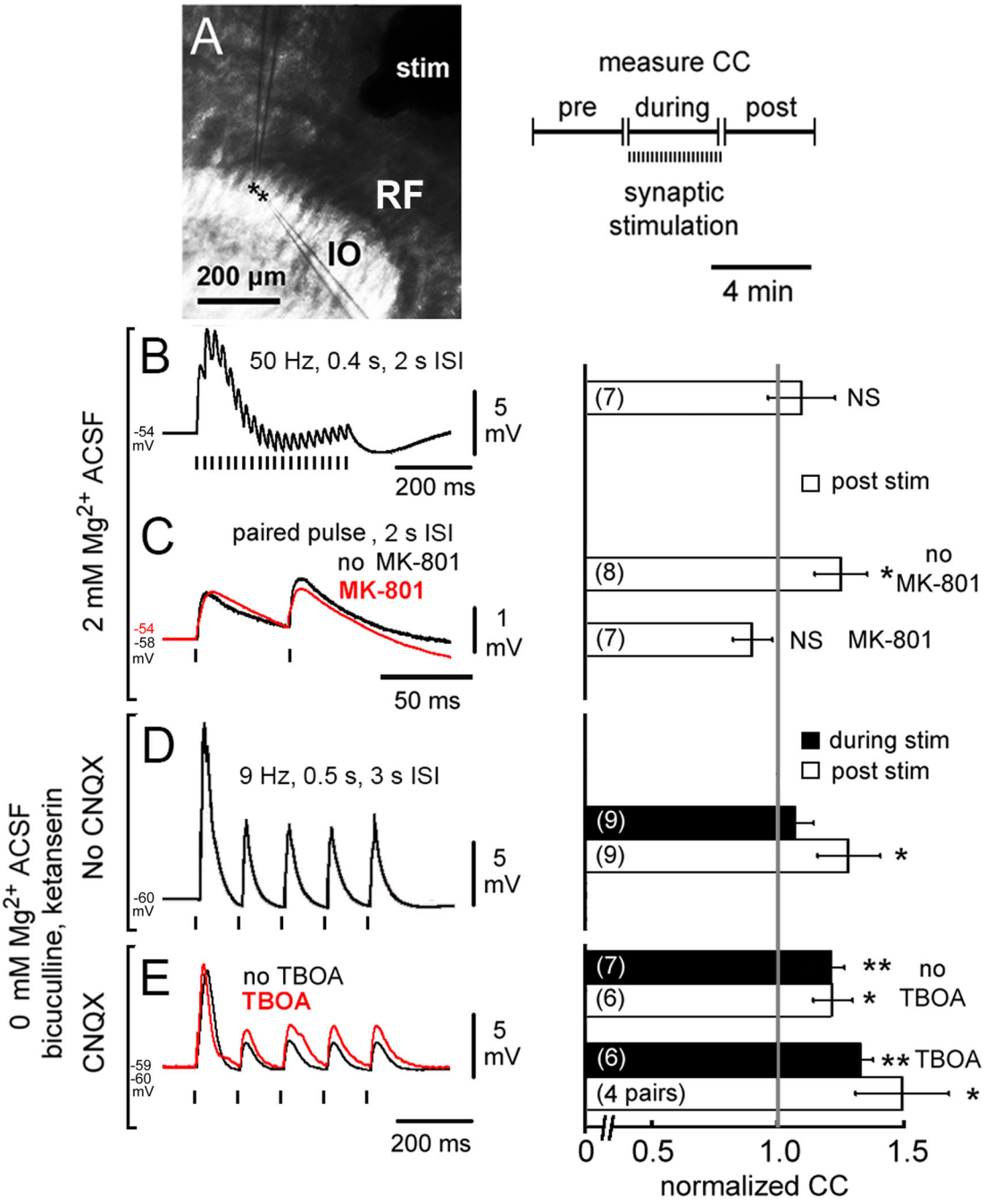

Figure 7. Synaptic activation strengthens electrical coupling

(A) Location of stimulating and recording electrodes and paradigm for measuring CCs (RF, reticular formation). (B–E) Effect of different stimulation paradigms on synaptic responses (left) and CCs (right, mean ± 1 SEM). 50-Hz stimulation bursts did not increase CC (B) while PPS strengthening of CCs (C, black) was occluded by MK-801 (C, red). 9-Hz stimulation in 0 Mg^{2+} ACSF during block of GABA and 5-HT receptors increased CCs at the completion of stimulation (D). Blocking AMPARs with CNQX (E, black) unmasked CC strengthening during 9-Hz stimulation and adding TBOA broadened EPSPs (E, red) and

amplified the synaptic strengthening of CCs (* $p < 0.05$, ** $p < 0.01$, ANOVA on ranks vs. normalized CC value of 1).

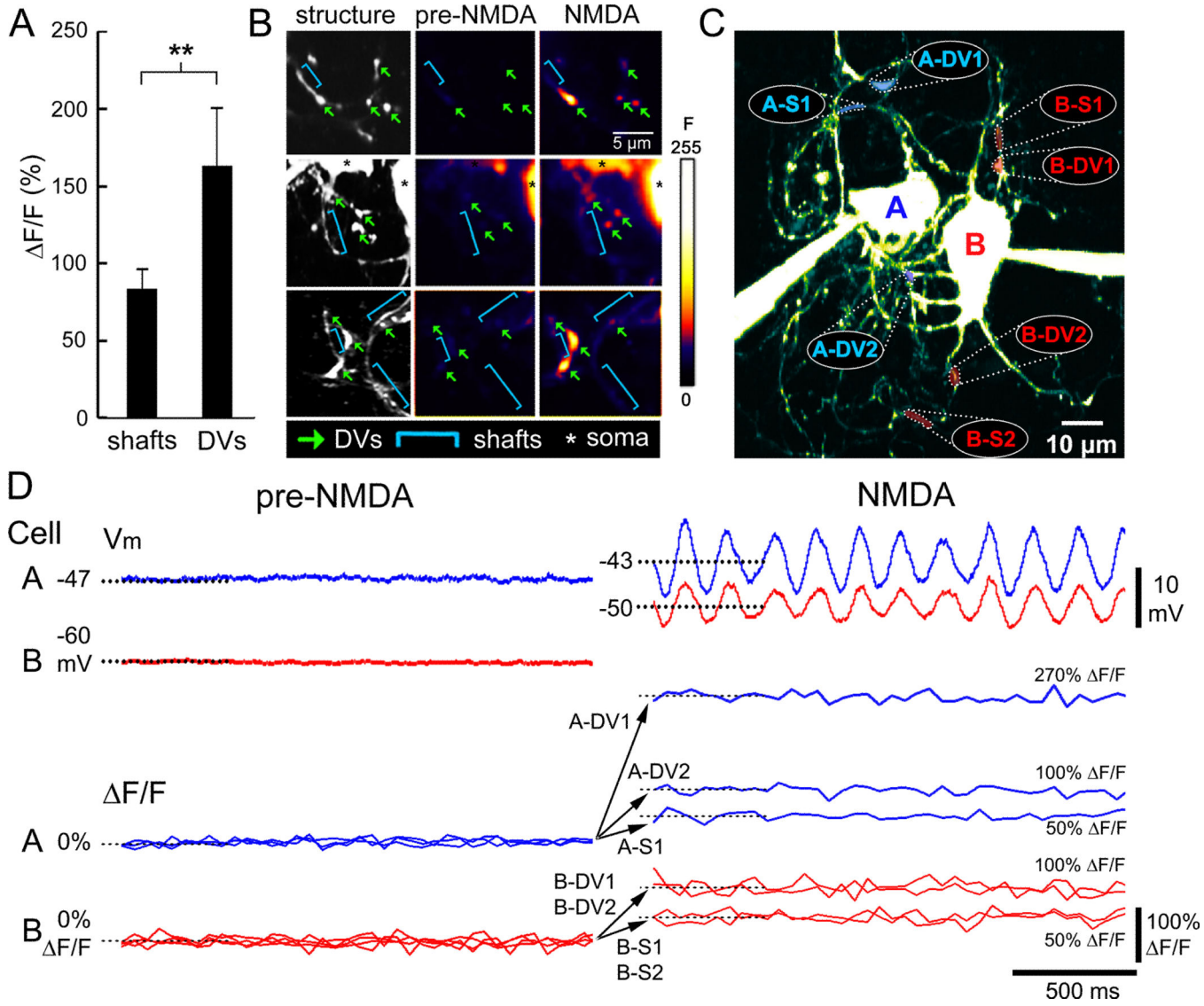

Figure 8. Ca^{2+} microdomains during STO synchronization in coupled IO neurons

(A) Mean (± 1 SEM) increase in ΔF/F evoked by NMDAR activation in dendritic shafts *vs.* DVs (**, $p < 0.05$, t-test). (B) 2-p imaging of 11 DVs (arrows) of electrically-coupled neurons demonstrate increased ΔF/F in DVs (arrows) but not dendritic shafts (brackets) by NMDAR activation. Images in (B) are single optical planes. (C) Axial projection of 2 electrically-coupled IO neurons (CC_{AB}=0.7%, CC_{BA}=1.8%) filled with Fluo-4 showing locations of simultaneous ΔF/F recordings (4 DVs, 3 shafts) during NMDAR activation. (D) Simultaneous records of somatic membrane potential and Ca^{2+} imaging at the dendritic loci in (C) demonstrate far greater increased ΔF/F in DVs than shafts during NMDAR induction of STO synchrony. See also Figure S5.